COMPUTER AIDED DESIGN STUDY OF HYPERMIXING NOZZLES

L. A. Mefferd and P. M. Bevilaqua
Rockwell International
Columbus Aircraft Division

- Abstract -

A combination of computer analysis and scale model testing was employed to compare the entrainment of the jets from a variety of lobe and swirl nozzles. The spreading of each jet was predicted with a finite difference solution of Reynolds' equations for the three-dimensional flow field. A two-equation turbulence kinetic energy model was used for closure. Limited experimental testing was then performed to verify the predicted trends. It was concluded that the largest increase in the entrainment rate can be obtained by increasing the length of the nozzle lobes, and that an alternating lobe nozzle yields the greatest entrainment for a given lobe size.

Sponsored by the Naval Air Systems Command, Contract N00019-77-C-0527.

INTRODUCTION

The U. S. Navy is studying several types of V/STOL aircraft for use with smaller carriers, as a more economical means of maintaining sea control. One way of obtaining the additional thrust required to give an aircraft V/STOL capabilities is by diverting the engine exhaust flow through a thrust augmenting ejector, as shown in Figure 1. An ejector is a kind of jet pump which utilizes entrainment by a stream of primary fluid to accelerate a larger mass of air drawn from the atmosphere. According to the laws of momentum and energy conservation for flow through the ejector, greater thrust is obtained by transferring the kinetic energy of the primary jet to the entrained air. A more complete description of this process has been given by Bevilaqua.[1]

The mechanism of this energy transfer is the turbulent mixing of the two streams. Thus, increases in the thrust augmentation of short ejectors can be obtained by increasing the rate of turbulent mixing. Significant gains in augmentation have been achieved in this way, with hypermixing[2,3] and lobed nozzles shown in Figure 2. The alternating jet segments of the hypermixing nozzle function like a series of jet flaps at the trailing edge of the nozzle. Streamwise vorticity, corresponding to the tip vortices of each jet flapped section of the nozzle, are shed into the flow between alternating sections. These vortices serve to accelerate the turbulent mixing and thus increase entrainment.

The lobe nozzle divides the jet into many thin sheets spread across the ejector inlet. In addition, cutting back the exit of the nozzle elements to form a kind of wedge, as shown in Figure 2, produces a pair of counter-rotating vortices at the ends of each jet segment. The roll up process is similar to the interaction which occurs for a jet in a cross flow.[4] This combination of jet furcation and vortex production generates approximately the same increase in mixing and entrainment as the hypermixing nozzle.

The objective of this study was to develop a nozzle which combines the hypermixing and lobe mechanisms to achieve further increases in jet entrainment and ejector performance. A previously developed computer program,[5] incorporating a two-equation turbulence model, was used to predict and compare the evolution of jets from various nozzle designs. Experimental testing was then used to verify predicted trends and to determine the actual performance of a nozzle developed from the analytic results.

METHOD OF ANALYSIS

Governing Equations

In order to predict the complex jet flap fields which develop from the nozzles to be studied, it is necessary to determine the solution for a turbulent, three-dimensional velocity and pressure field. Considerable savings in computer storage and running time were achieved by utilizing a procedure developed by Patankar and Spalding[6] to reduce solution of the three-dimensional problem to the solution of a series of two-dimensional

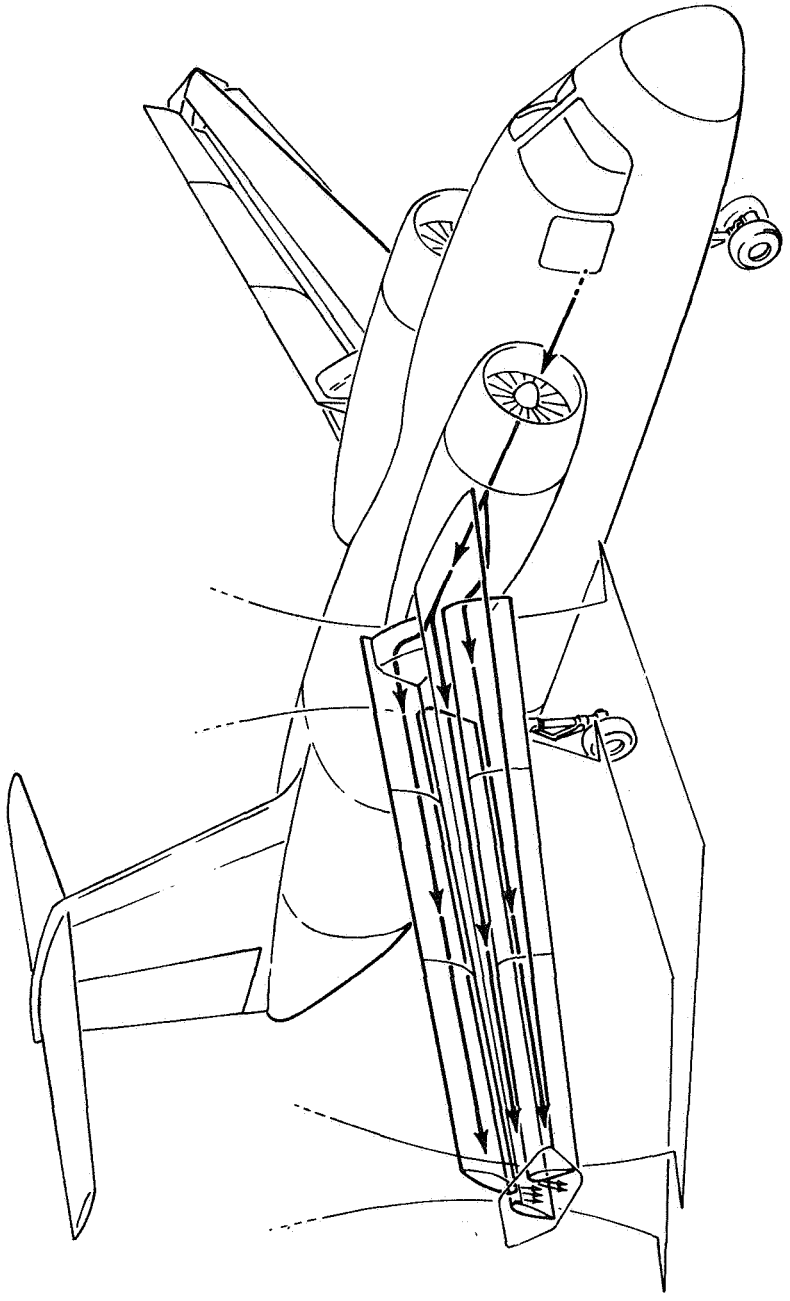

Figure 1. Ejector Wing V/STOL Aircraft.

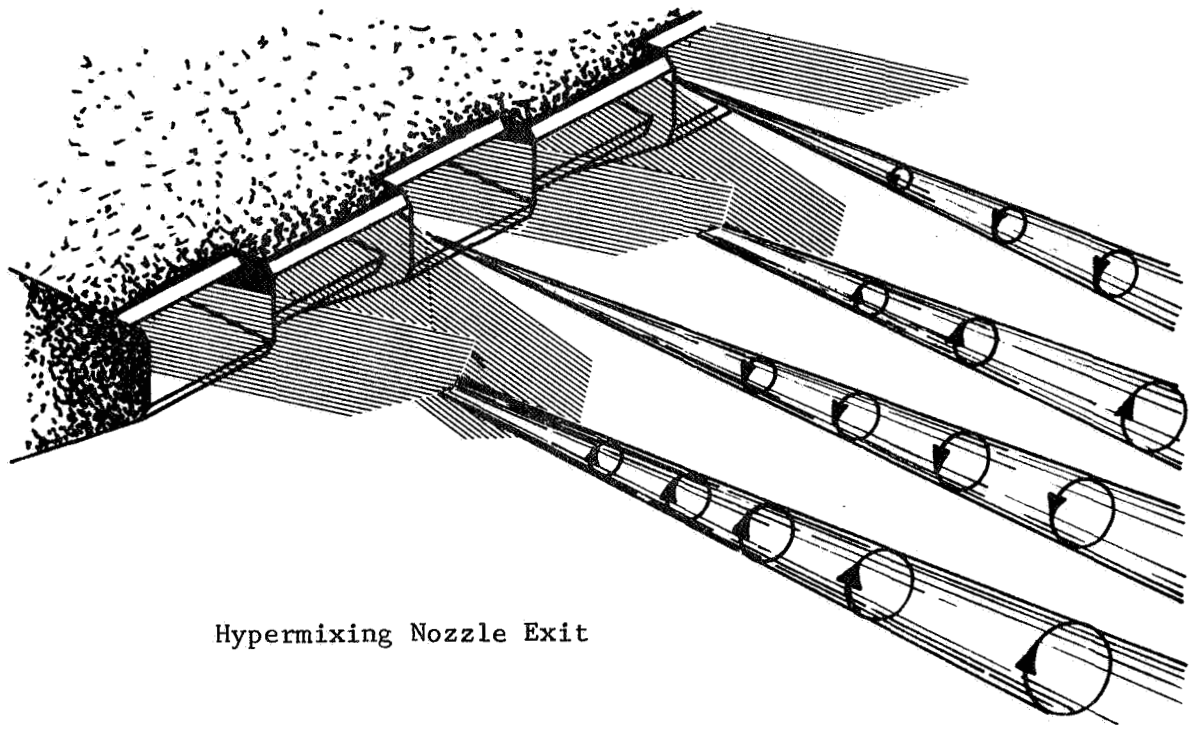

Hypermixing Nozzle Exit

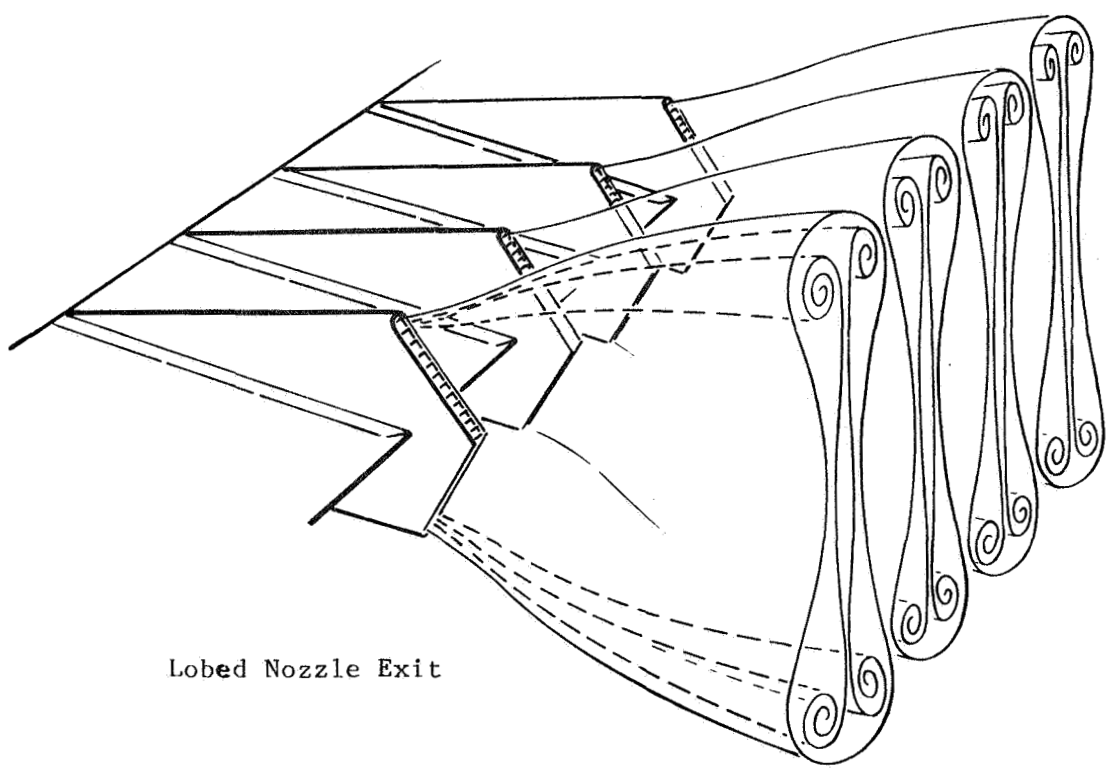

Lobed Nozzle Exit

Figure 2. Baseline Nozzles.

problems. Since there is a primary direction of flow (through the ejector), a thin shear layer approximation was applied. The gradients of the normal stress are thus neglected, and the streamwise velocity component is considered to be "driven" by a mean pressure $\overline{p}(x)$, which is decoupled from the perturbation pressures $p'(x,y,z)$ in the transverse planes. An additional assumption that the fluid density is constant was also made. These assumptions reduce the governing fully elliptic equations to a set which is parabolic in the streamwise direction, but elliptic in places across the flow. In Cartesian coordinates, the equations for the conservation of mass and momentum become

Continuity

$$\frac{\partial u}{\partial x} + \frac{\partial v}{\partial y} + \frac{\partial w}{\partial z} = 0 \tag{1}$$

Momentum

$$\rho u \frac{\partial u}{\partial x} + \rho v \frac{\partial u}{\partial y} + \rho w \frac{\partial u}{\partial z} = \frac{\partial \tau_{yx}}{\partial y} + \frac{\partial \tau_{zx}}{\partial z} - \frac{d\overline{p}}{dx} \tag{2}$$

$$\rho u \frac{\partial v}{\partial x} + \rho v \frac{\partial v}{\partial y} + \rho w \frac{\partial v}{\partial z} = \frac{\partial \tau_{yy}}{\partial y} + \frac{\partial \tau_{zy}}{\partial z} - \frac{\partial p'}{\partial y} \tag{3}$$

$$\rho u \frac{\partial w}{\partial x} + \rho v \frac{\partial w}{\partial y} + \rho w \frac{\partial w}{\partial z} = \frac{\partial \tau_{yz}}{\partial y} + \frac{\partial \tau_{zz}}{\partial z} - \frac{\partial p'}{\partial z} \tag{4}$$

Here, u, v, w are the time averaged velocity components and the τ_{ij} are the turbulent shear stresses.

The turbulent stresses are calculated using the two-equation turbulence model of Launder and Spalding.[7] An eddy viscosity assumption is used to relate the stresses to the velocity gradients. The expression in Cartesian tensor notation is:

$$\tau_{ij} = \mu_t \left(\frac{\partial u_i}{\partial x_j} + \frac{\partial u_j}{\partial x_i} \right) - \frac{2}{3} \rho k \delta_{ij} \tag{5}$$

where δ_{ij} is the Kronecher delta, and k is the kinetic energy of turbulence. For the parabolic flow considered here, the velocity gradients in the x-direction (i.e., $\partial u_i / \partial x_1$) will be neglected. The eddy viscosity μ_t is calculated from the turbulent kinetic energy and its rate of dissipation, ϵ. The expression for μ_t is

$$\mu_t = c_\mu \rho k^2 / \epsilon \tag{6}$$

in which c_μ is a constant of proportionality.

The equations for k and ϵ are

$$\rho u \frac{\partial k}{\partial x} + \rho v \frac{\partial k}{\partial y} + \rho w \frac{\partial k}{\partial z} = \frac{\partial}{\partial y}\left(\frac{\mu_t}{k}\frac{\partial k}{\partial y}\right) + \frac{\partial}{\partial z}\left(\frac{\mu_t}{k}\frac{\partial k}{\partial z}\right) + G - \rho\epsilon \tag{7}$$

$$\rho u \frac{\partial \epsilon}{\partial x} + \rho v \frac{\partial \epsilon}{\partial y} + \rho w \frac{\partial \epsilon}{\partial z}$$

$$= \frac{\partial}{\partial y}\left(\frac{\mu_t}{\sigma\epsilon}\frac{\partial \epsilon}{\partial y}\right) + \frac{\partial}{\partial z}\left(\frac{\mu_t}{\sigma\epsilon}\frac{\partial \epsilon}{\partial z}\right) + (c_1 G - c_2 \rho\epsilon)\left(\frac{\epsilon}{k}\right) \tag{8}$$

The quantity G is the rate of generation of k by the action of velocity gradients. Since, in the present situation, the only significant gradients are $\partial u/\partial y$ and $\partial u/\partial z$, the expression for G becomes

$$G = \mu_t \left[\left(\frac{\partial u}{\partial y}\right)^2 + \left(\frac{\partial u}{\partial z}\right)^2\right] \tag{9}$$

The turbulence model involves five empirical constants. According to the recommendation of Launder and Spalding,[7] the following values of the constants are used:

c_μ	c_1	c_2	σ_k	σ_ϵ
0.09	1.44	1.92	1.0	1.3

Thus, the turbulence constants were not adjusted for the present case.

These equations were put in finite difference form by integrating them over a control volume surrounding each grid point in the domain of solution. The resulting non-linear equations are linearized by using upstream values of the flow variables to evaluate the cross stream convection and diffusion coefficients. The equations are solved by the use of a tri-diagonal matrix algorithm. From known conditions at an upstream cross section, x, the flow field at the downstream cross section, $x + \Delta x$, is computed. This streamwise marching process is continued until the domain of interest has been covered. A more complete description of this program and an illustration of its use were given by Patankar and DeJoode.[5]

Boundary Conditions

The computational boundaries for representative nozzles are outlined with dashed lines in Figure 3. Although the jets are three-dimensional, the ejector shroud is two-dimensional, so that there is no change in the chordwise dimension, y, with respect to the spanwise dimension, z. Symmetry planes were used as computational boundaries in the spanwise direction, because most nozzle designs are periodic along the span. That is, there are no physical endwalls. The velocity normal to the symmetry planes is zero, and the normal gradients of other flow variables are also zero at these planes.

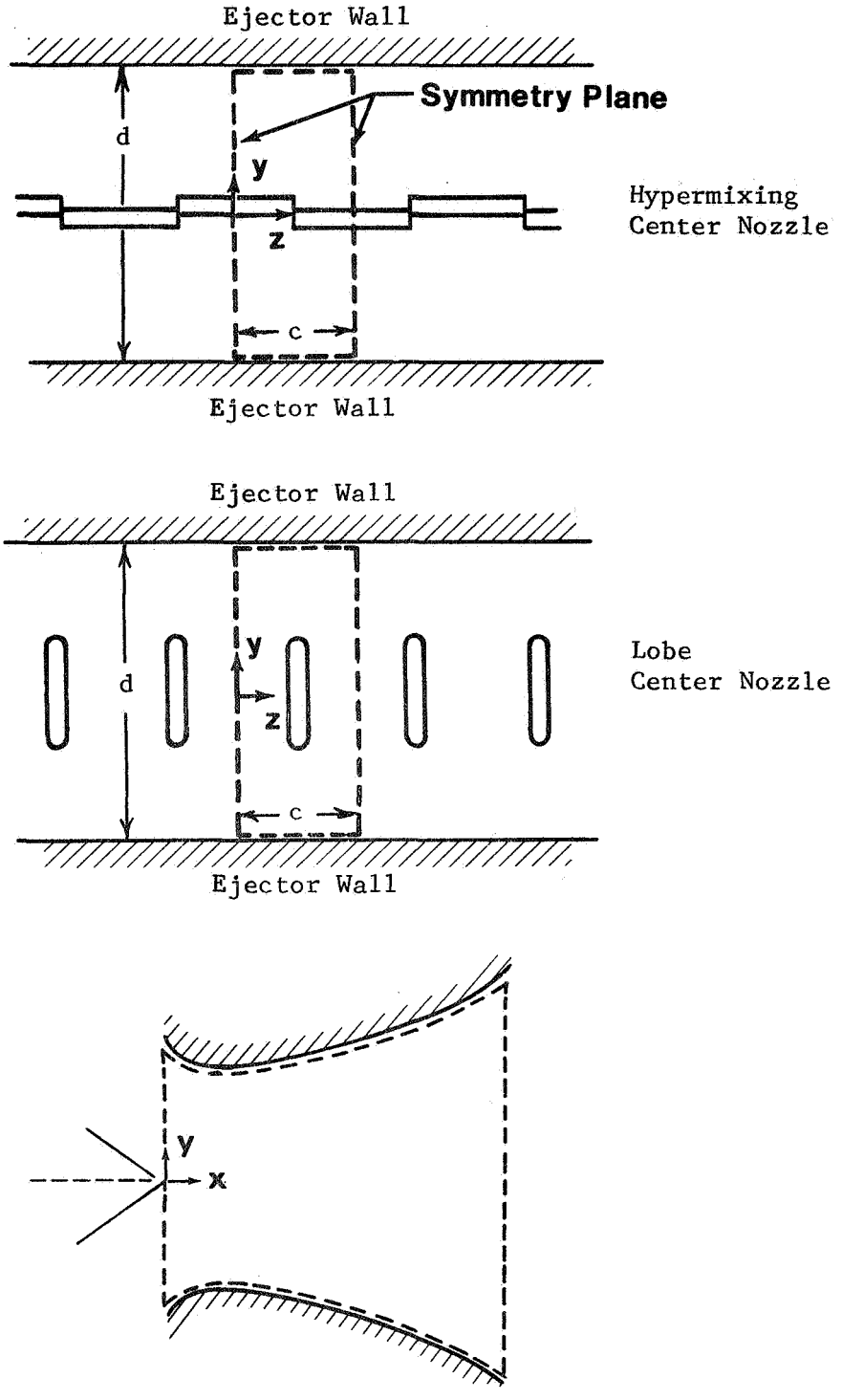

Figure 3. Computational Boundaries for Representative Nozzles.

The nozzles were compared by calculating their performance in an ejector representative of an average between the wing and canard on the XFV-12A ejector wing technology demonstrator aircraft.[8] The parameters used were an inlet area ratio of 13, diffuser length/throat width ratio of 2.0, diffuser area ratio of 1.8, and a flow split of 55% to the central nozzle. Although the performance of the nozzles depends to some extent on the ejector configuration, it was felt that conclusions regarding the relative performance of alternate nozzle concepts could be generalized for this type of ejector.

Initial Conditions

Solution of the ejector equations has thus been transformed to an initial value problem which is solved by streamwise integration. Initial values of all the flow variables must therefore be specified in order to start the calculation. Because there was no data available for the new nozzle concepts, experience with previously tested hypermixing and lobe nozzles was utilized to make reasonable assumptions for the initial conditions. The initial jet velocity of each nozzle was calculated by multiplying the isentropic velocity computed for the nozzle pressure ratio by an appropriate velocity coefficient, $C_V \equiv V_{actual}/V_{isentropic}$. The same value of this coefficient was used for every nozzle; that is, it was assumed that the internal viscous losses were the same for every nozzle. A value of $C_V = 0.925$ was chosen. The stagnation pressure, $P_S/P_{atm} = 2.1$, and temperature, $T_S = 550°R$, were chosen as typical of the primary jets of laboratory ejectors. Some deflection of the jet is utilized in each of the nozzles to promote vortex formation. The resultant tilt loss in the jet thrust was included by inclining the initial jet velocity vector at the appropriate deflection angle. Thus, the predictions of ejector performance balance the tilt loss in jet thrust against the associated increase of entrainment. Each of the nozzles had the same exit area and the same mass flow.

The wall jets were specified as being tangent to the surface of the inlet contraction, which made a 30° angle with the ejector axis. No corrections were made to the turbulence model or the momentum equations to account for the effect of wall curvature on these jets. The entrainment and thrust of the wall jets were therefore underpredicted, but since this treatment was the same in every case, the comparison of the central nozzles should not have been affected.

The initial turbulence intensity was not measured in any of the previous experiments. However, sensitivity studies performed by DeJoode and Patankar[5] showed that the development of the velocity profiles was relatively insensitive to probable variations in the initial turbulence level. This is because the hypermixing vortices dominate the turbulent processes. For the present analysis, the initial turbulence kinetic energy in the jet was specified to be 6% of the jet energy. In the secondary stream the turbulence energy was set equal to 0.01% of the stream energy. Similarly, the initial level of turbulence dissipation did not have a significant effect on the jet development. An initial value of $\epsilon = 0.13\ U_o^3/t$, where t is the initial nozzle gap, was chosen as being typical of the jets previously tested.

Evaluation of the Thrust Augmentation

The thrust augmentation ratio is defined to be the ratio of the ejector stream thrust to the isentropic thrust obtained by expanding the same mass of primary fluid to atmospheric pressure. The thrust of the ejector is evaluated by integrating the thrust of the mixed flow at the ejector exit. It is given by

$$T_e = \int_{A_3} \rho u^2 dy\, dz - (P_{atm} - P_3)A_3 \qquad (10)$$

in which u is the mainstream velocity, and P_3 and A_3 are the static pressure and area at the exit. The static pressure is assumed constant at the exit. It should be noted that even though the pressure force is negative, the reduced exhaust pressure results in a net thrust increase because the momentum flux is increased more than the pressure force is reduced.

NUMERICAL PREDICTIONS

In order to illustrate the predictions of the computer program and provide a baseline level of performance, the jets from representative hypermixing and lobed nozzles were examined. Development of the jets from these nozzles are shown in Figures 4 and 5. In each figure the axial velocity profiles at three streamwise stations corresponding to the ejector throat, a point midway through the diffuser, and the ejector exit are shown on the left. The convection velocities in the transverse planes at the first two stations are shown on the right. Note that the spanwise scale along the base of the axial velocity profiles has been elongated to show details. The location of the grid points is the same for the axial and transverse velocity profiles at each station. In the transverse planes, each velocity vector is centered on a grid point; the surface of the axial velocity profiles is defined by lines passing over these points. A sketch of the nozzle exit is shown at the bottom of the page. To simplify making comparisons, these same profiles will be shown for every nozzle.

In Figure 4 the hypermixing jet runs along the span on the centerline. There is a wall jet on each side of the hypermixing jet, and the relative magnitude of the secondary velocity is seen in the region between the primary jets. At the throat station, the displacement of adjoining segments of the hypermixing jets is apparent in the axial profiles, while the streamwise vortex can be seen in the transverse plane. The rotation of the vortex convects each jet segment around and behind the adjoining segment, as seen at the second station. This produces a characteristic double peak in the chordwise velocity profiles. Continued mixing acts to merge these peaks and broaden the profiles, as seen at the exit station. The thrust augmentation ratio, defined as the ratio of the exit momentum flux to the isentropic thrust of the primary jets, was predicted to be $\phi = 1.37$ for this nozzle. By comparison, the augmentation predicted for an ordinary slot nozzle is $\phi = 1.20$.

Axial Velocities

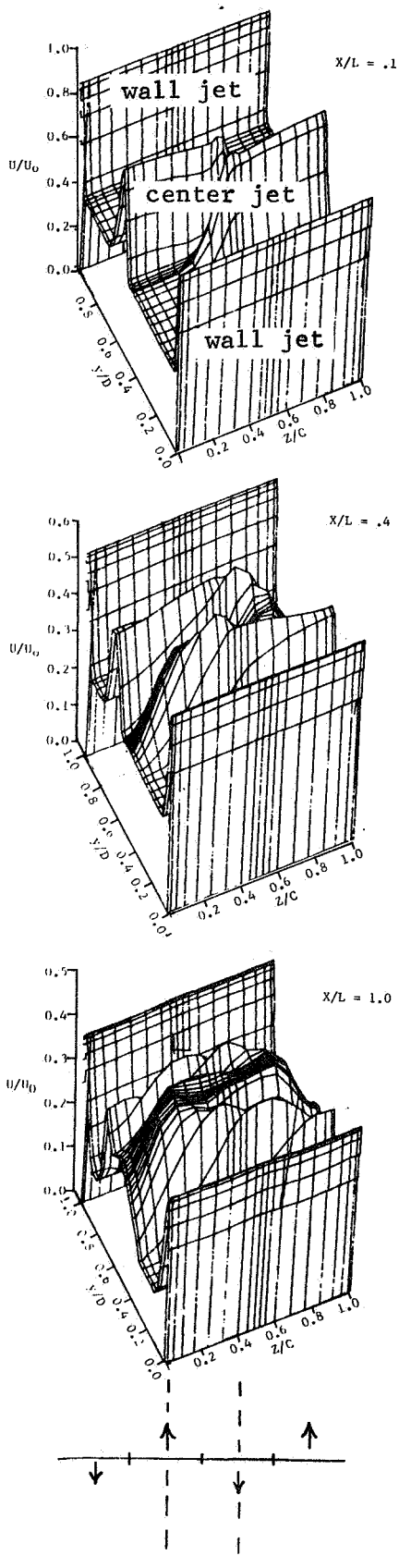

Convection Velocities

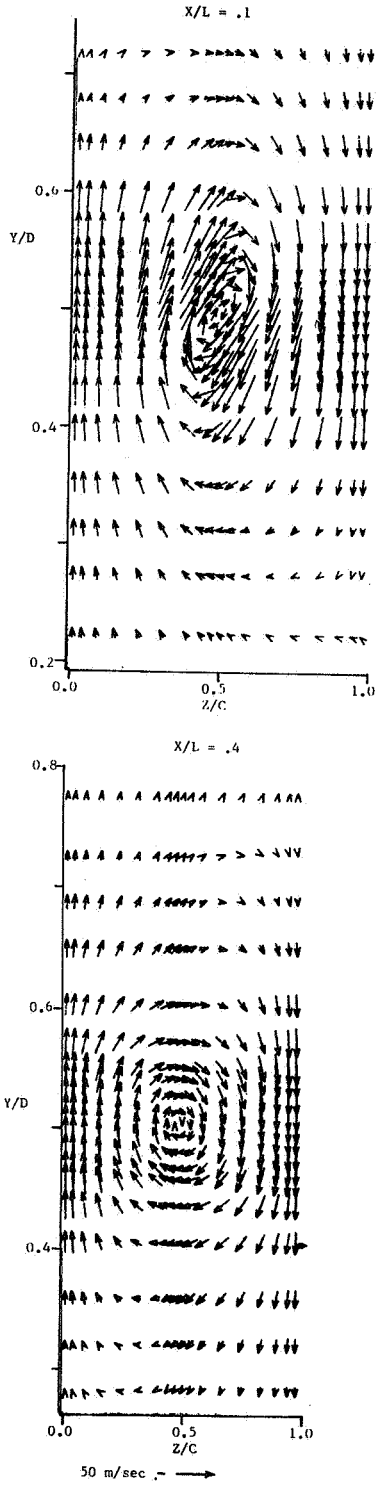

Figure 4. Baseline Hypermixing Nozzle, Ø = 1.37.

Development of the jet from the lobe nozzle is shown in Figure 5. The nozzle gap is the same as for the hypermixing jet and the length of each lobe is one-fourth of the ejector throat width. In the figure the left hand symmetry plane runs through the center of the segment so that only half of the jet is seen. The pair of counter-rotating vortices are at the ends of each segment. The mixing action of these vortices produces a local increase in the entrainment, and this causes the jet to develop the "dog bone" shaped cross section seen in the figure. The augmentation in this case is $\phi = 1.34$.

The jets from more than two dozen new nozzles were examined during the study. The basic nozzle consists of alternating crosswise and spanwise lobes. Only a few representative configurations will be discussed here. The nozzle shown in Figure 6 has a lobe positioned between the hypermixing vortices. In the figure the hypermixing vortex is at the center and the vortex pair eddies are on the sides. The velocities induced by the vortex pairs reinforce the hypermixing velocities on the diagonal running from lower left to upper right, but oppose them on the other diagonal. Comparison of the exit velocity profile with those of the baseline nozzles reveals that this interaction reduces the spreading of the hypermixing segment. However, the addition of the nozzle lobes increases the net entrainment and the thrust augmentation ratio is increased to $\phi = 1.41$.

For the nozzle shown in Figure 7, alternate sides of each lobe were deflected in opposite directions. Three streamwise vortices develop in this case. The central vortex is twice as strong as either tip vortex, since it is formed by combination of the two root vortices. The vortex pair eddies do not appear because there is no chordwise deflection of the jet. The rotation of the central vortex can be seen to drive the jets from adjacent lobes together at the symmetry planes. This limits the entrainment of these jets, leaving a large unmixed region between the merged jets. As a result, the augmentation ratio was reduced to $\phi = 1.26$ with this nozzle.

A composite nozzle in which the lobe vortex is centered over the hypermixing vortex is shown in Figure 8. The lobe vortex and the tip vortex on each side of it rotate in the same direction, so that they coalesce to form the single vortex seen in the figure. There is additional entrainment associated with this process, and the thrust augmentation ratio is increased over the previous nozzle. However, the lobe jet is rotated into the spanwise jet in this case also, and the augmentation ratio is only increased to $\phi = 1.31$.

In the last nozzle shown, the length of the lobe is equal to the ejector throat width. The development of the axial velocity profiles for one of the jets is shown in Figure 9. In this orientation the spreading of each jet is greater than if it were aligned with the ejector span, because the mean jet vorticity is stretched as it passes through the diffuser. Vortex stretching is the primary mechanism of turbulent energy dissipation[9] and entrainment is associated with this dissipation. It can be seen that adjacent jets have just merged with each other by the ejector exit. The augmentation ratio was increased to $\phi = 1.61$ with this configuration. A description of the predicted results for other nozzle configurations may be found in the contract report.[10]

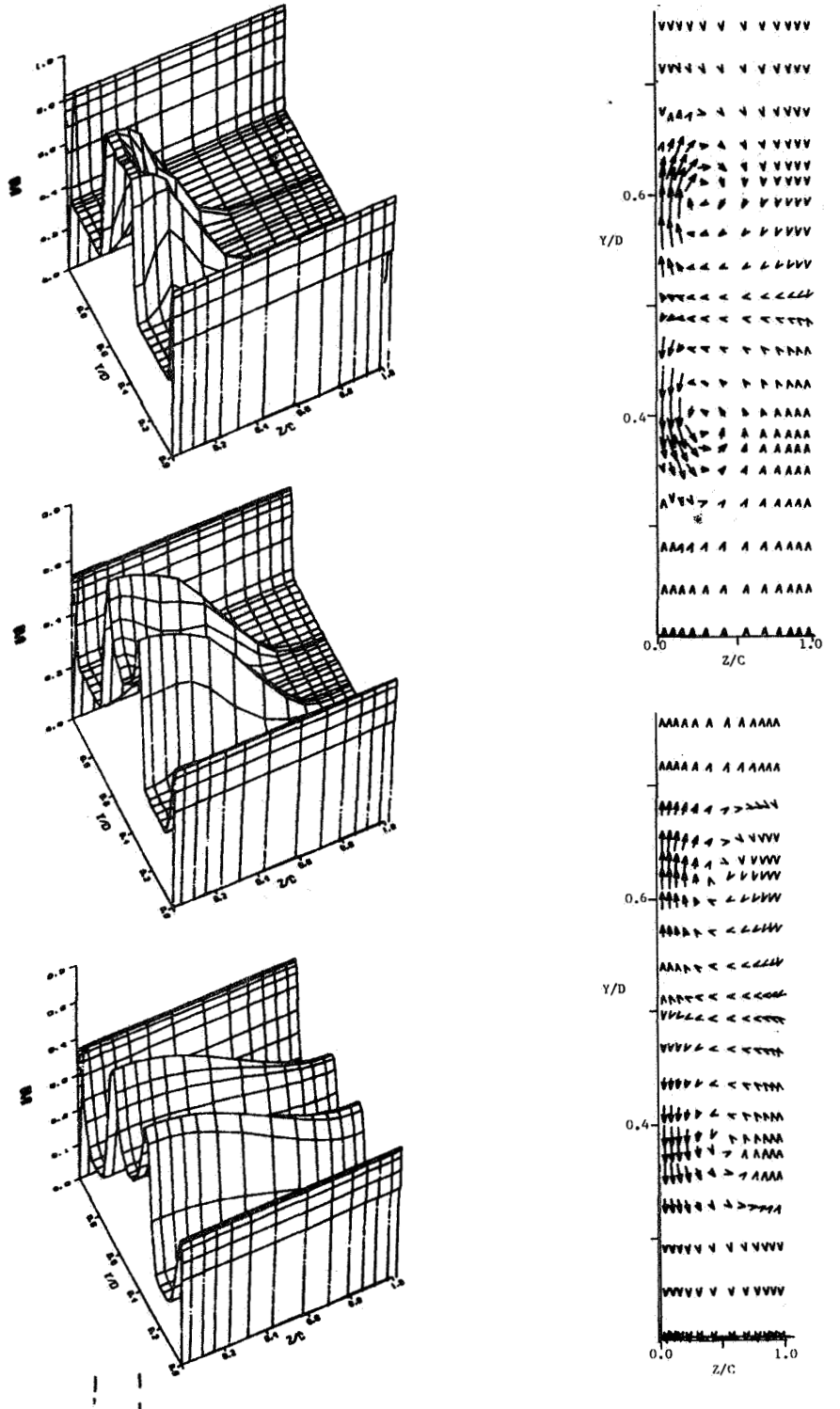

Figure 5. Baseline Lobe Nozzle, Ø = 1.34.

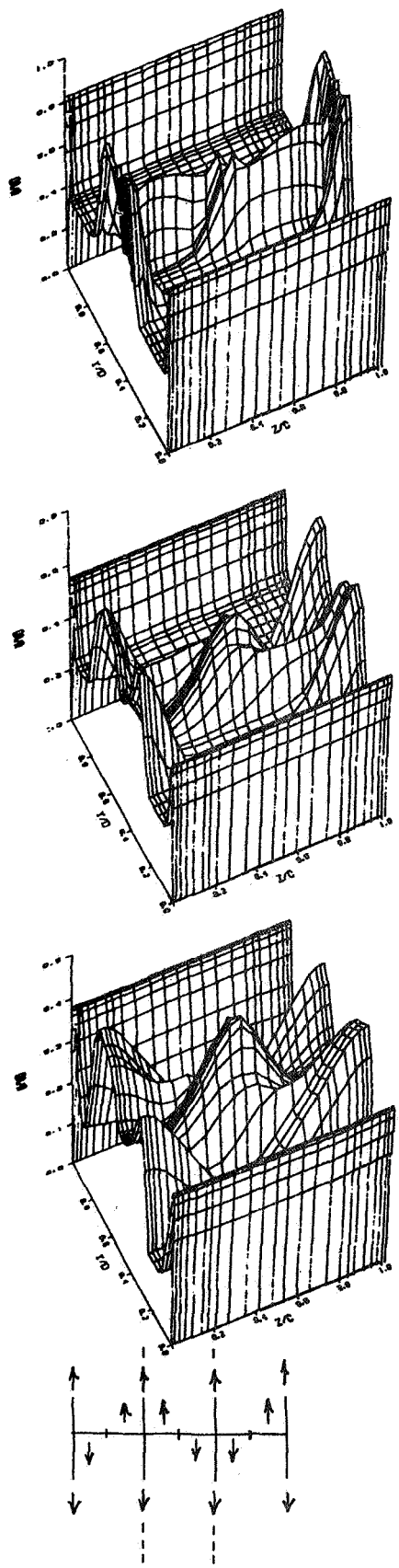

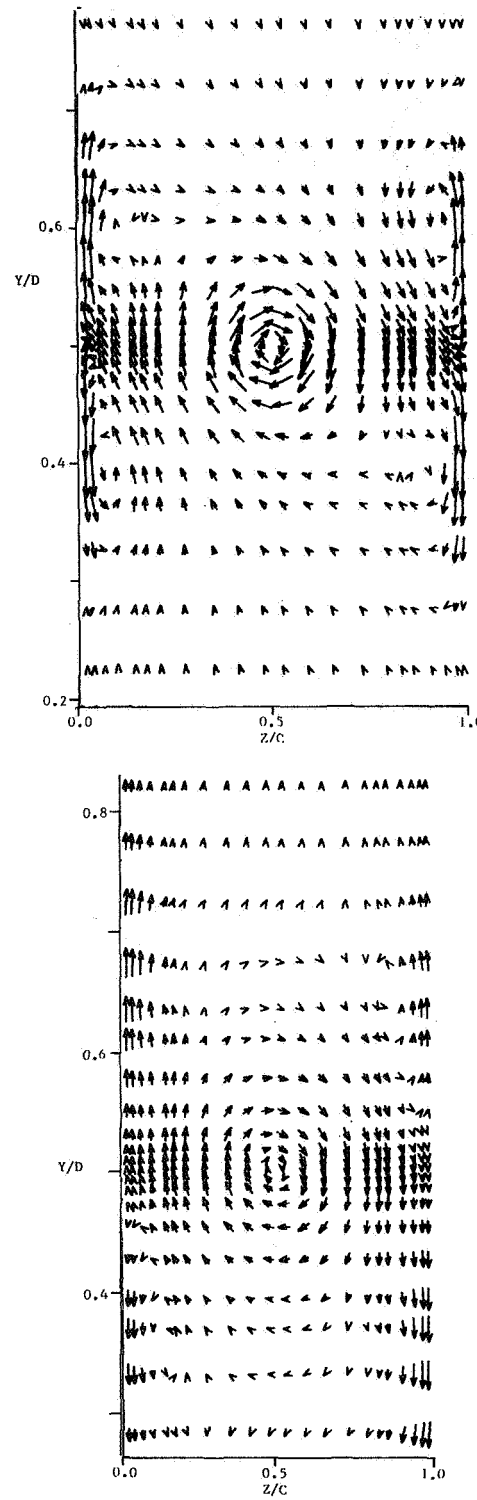

Figure 6. Vortex Centered Between Crosswise Lobes, Ø = 1.41.

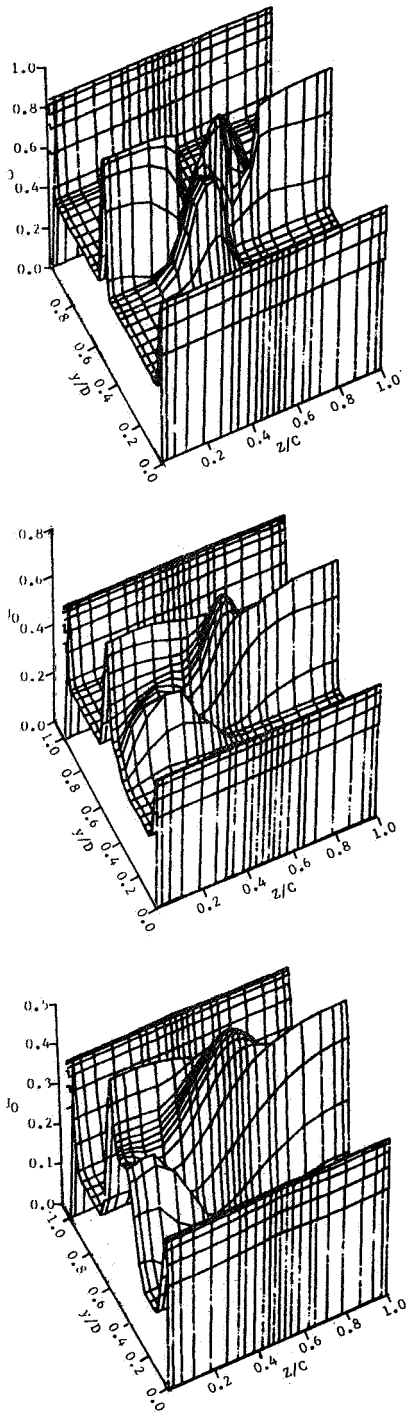

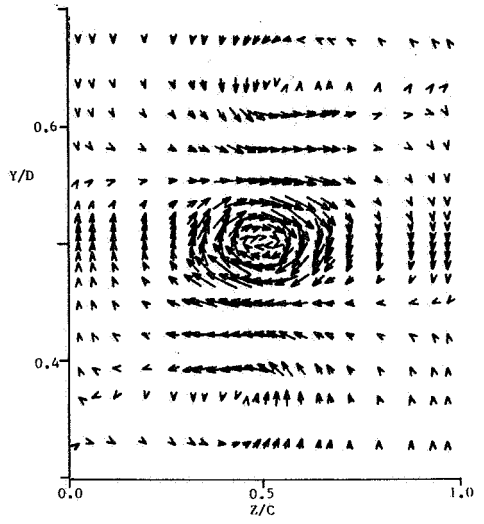

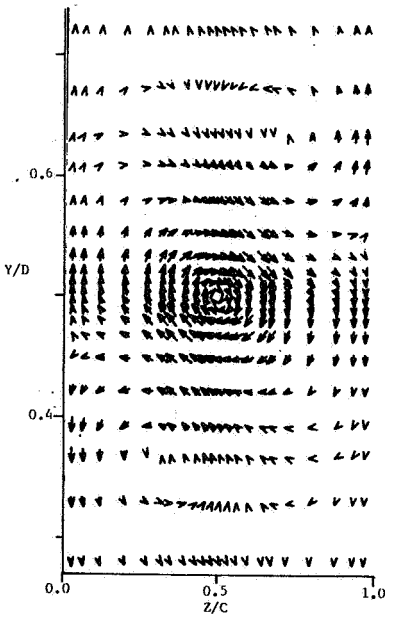

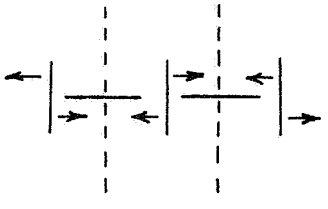

Figure 7. Vortex Centered on Lobes with No Wedge Angle, Ø = 1.26.

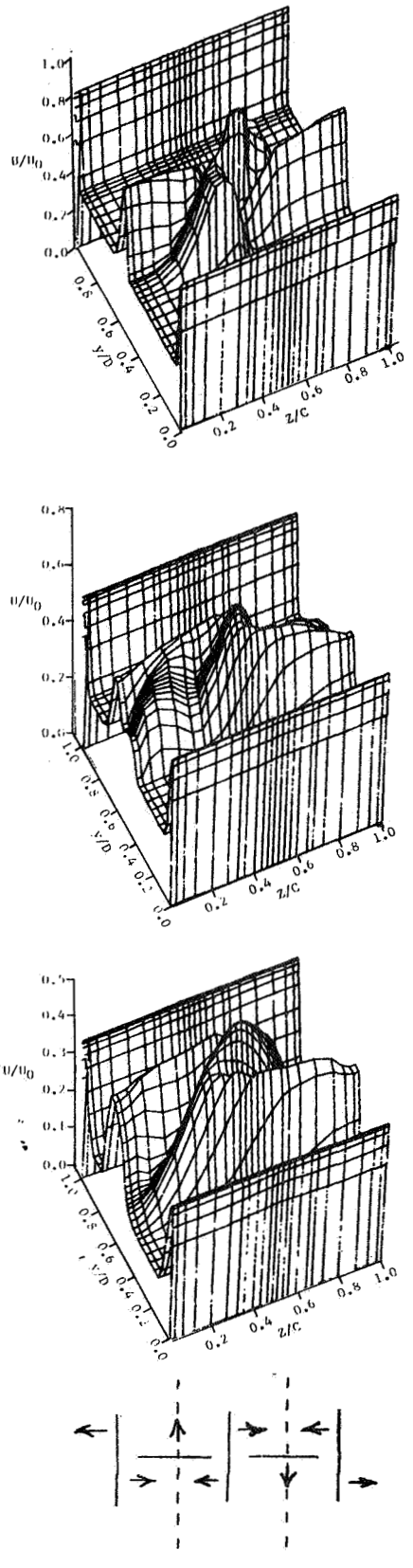

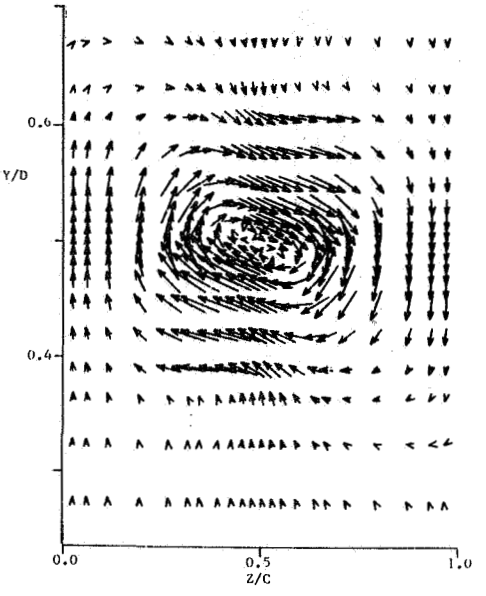

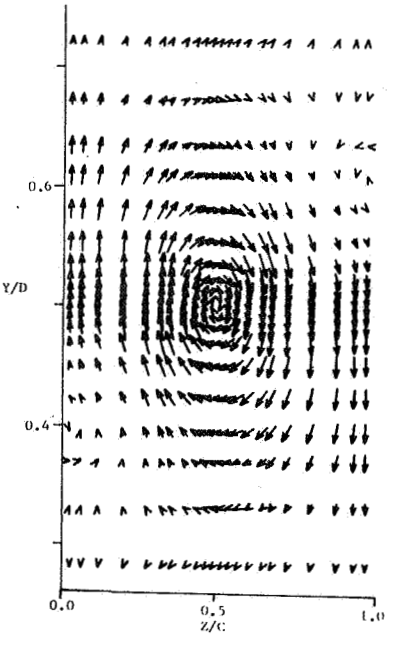

Figure 8. Crosswise Lobe Vortex Centered over Hypermixing Vortex, Ø = 1.31.

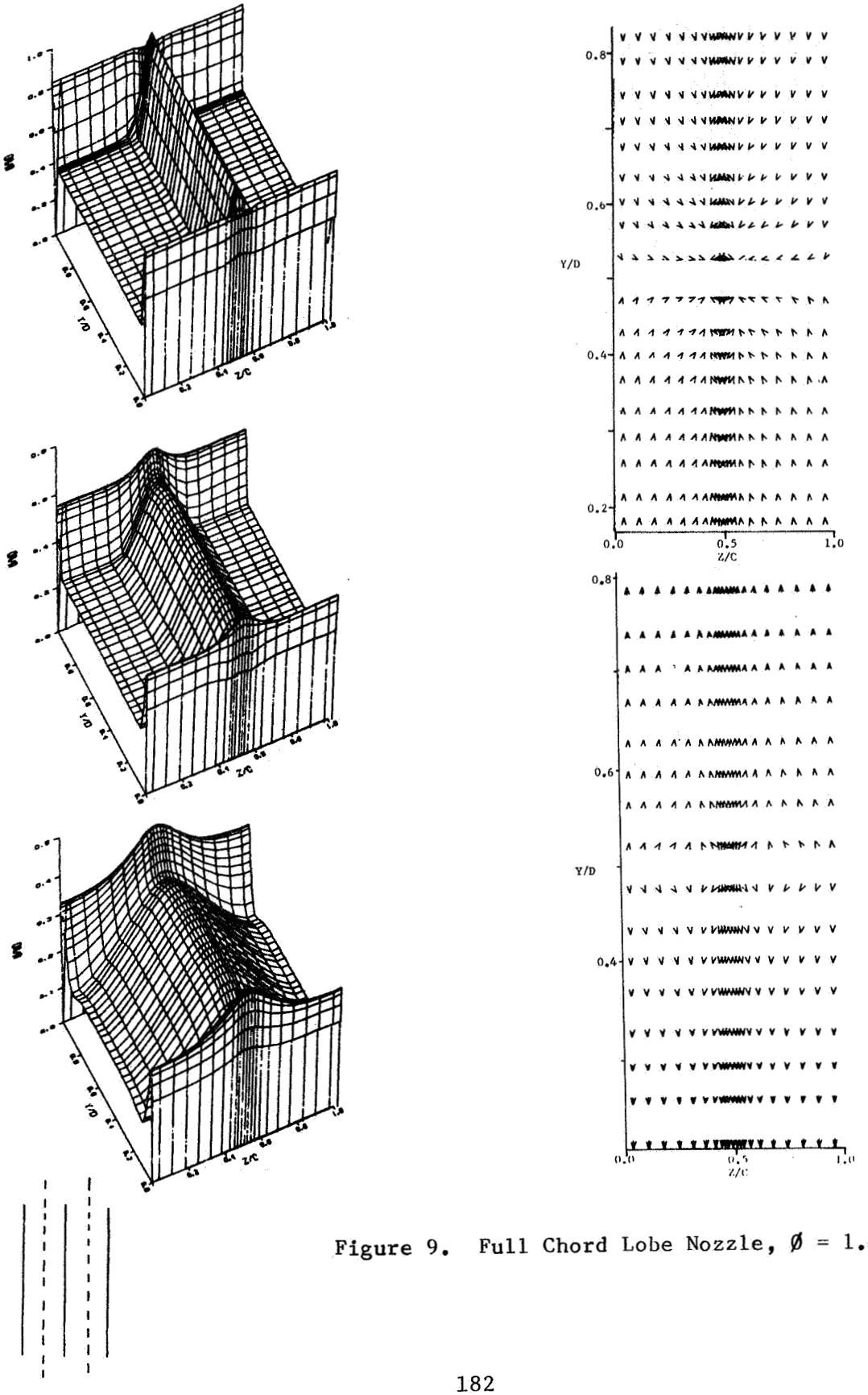

Figure 9. Full Chord Lobe Nozzle, Ø = 1.61.

EXPERIMENTAL RESULTS

Limited experimental testing was performed to verify the predictions that the addition of a vortex to a short lobe reduces the augmentation, but that the addition of a vortex between the lobes increases the augmentation. In the interest of economy, these tests were performed in an existing ejector model. The model was mounted on a cradle suspended on four cables attached to a fixed frame. The ejector thrust was measured with load cells installed between the cradle and frame. High pressure air was supplied to the primary nozzles through flexible hoses. The isentropic reference thrust was calculated from the measured primary flow and the nozzle exit pressure.

The effect of the lobe vortex was determined by direct comparison; the hypermixing lobe nozzle was constructed by cutting back opposite sides of the lobes on the reference nozzle. Each nozzle was installed in the ejector, and the thrust augmentation ratio was measured over a range of diffuser area ratios. As shown in Figure 10, the peak augmentation ratio was significantly reduced by the addition of the vortex. A hot wire anemometer was used to obtain midspan velocity profiles at a diffuser area ratio of 1.8, for both nozzles. The measured profiles matched the predicted profiles well, verifying the mechanism of the thrust loss. Thus, the prediction that the vortex reduced the augmentation by driving adjacent lobes together was confirmed.

In the second series of tests, the prediction that a vortex between the lobes increases the augmentation was verified. Since an existing hypermixing nozzle was the baseline in this case, another ejector was used for these tests. The measured thrust augmentation of $\phi = 1.54$ represents an improvement over the $\phi = 1.49$ attained with the hypermixing nozzle (Figure 11). The development of the profiles was the same as the numerical predictions. Thus, the analytic predictions were verified in this case also. The wide lobe nozzles were not tested because considerable development work has already been carried out in this case.[11]

CONCLUSIONS

There are two major conclusions of this study. First, the partially parabolic solution procedure can be used to predict the development of these highly three-dimensional jets. To our knowledge, this is the first time the method has been utilized in this way. We did not notice the sensitivity to initial turbulence properties sometimes noted as a deficiency of the method. The probable reason is that the large vortices dominate the turbulent processes. The second conclusion is that the hypermixing and lobe nozzles are not readily combined. Nevertheless, significant gains in augmentation can be achieved with nozzles developed by numerical analysis.

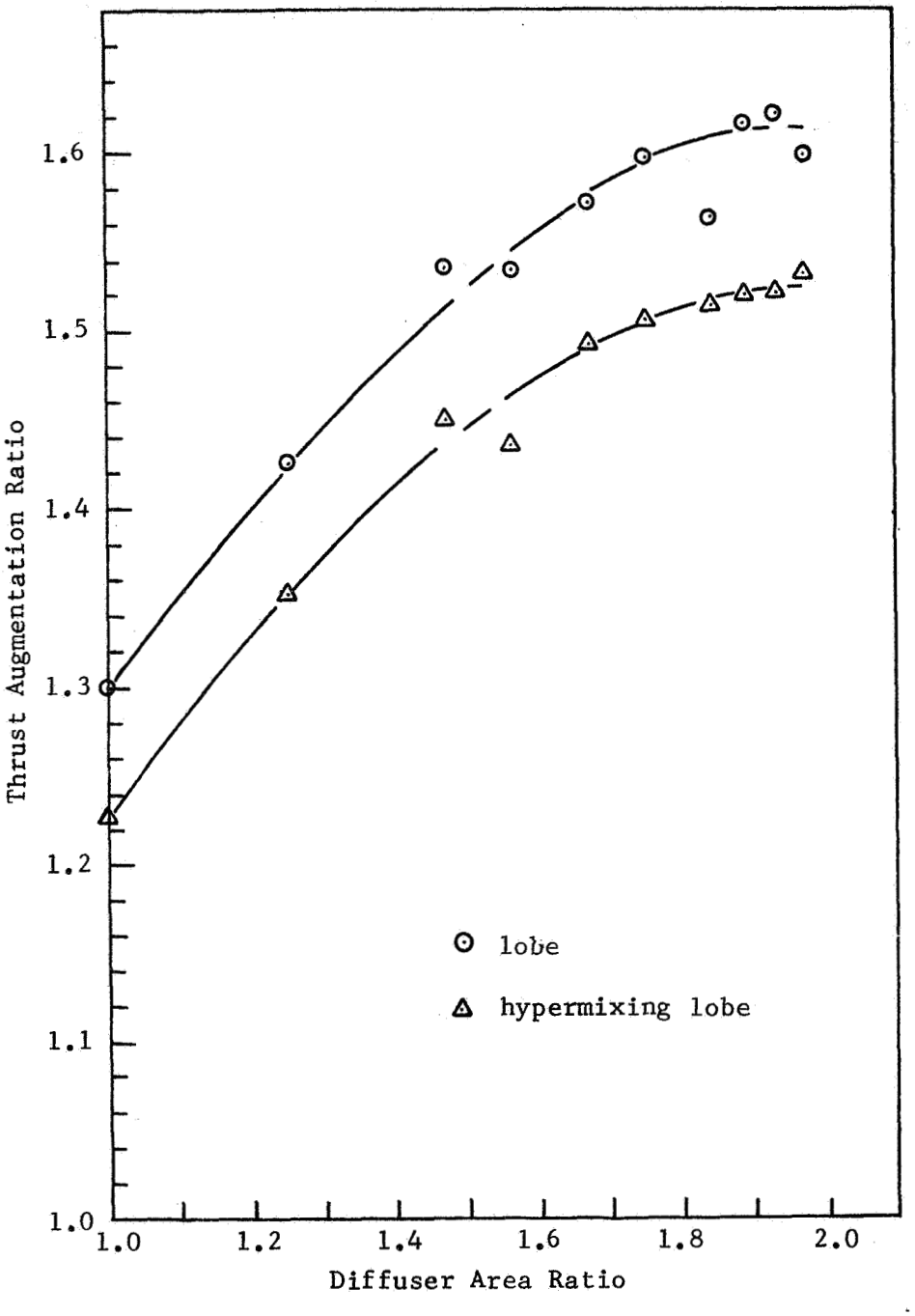

Figure 10. Effect of Hypermixing on Thrust Augmentation of Lobe Nozzles.

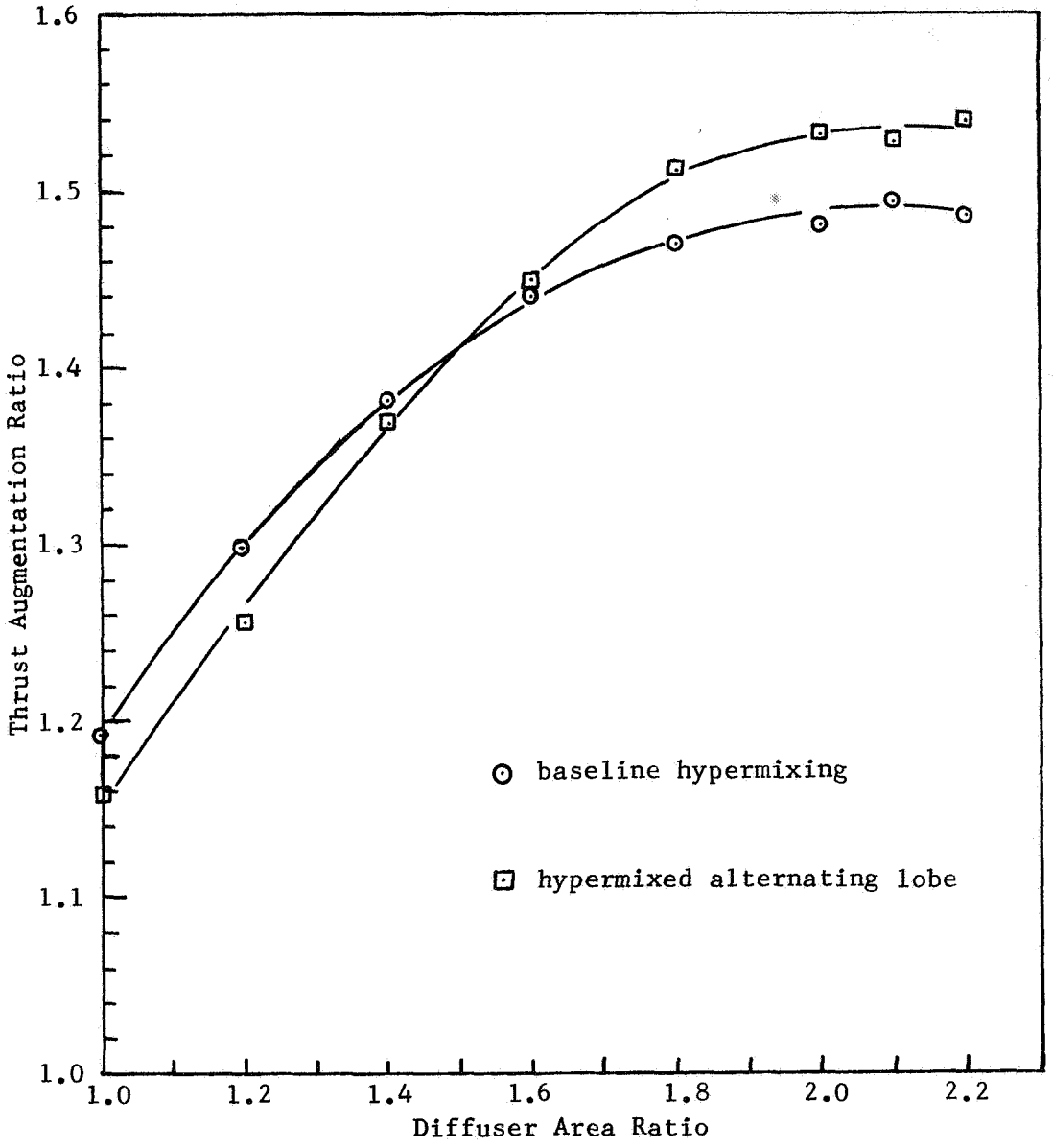

Figure 11. Comparison of Thrust Augmentation for Hypermixing Nozzle and Nozzle with Vortex Centered Between Lobes.

REFERENCES

1. Bevilaqua, P. M., "Lifting Surface Theory for Thrust-Augmenting Ejectors," AIAA Journal, Vol. 16, No. 5, May 1978, pp. 475-481.

2. Quinn, B. P., "Compact Ejector Thrust Augmentation," Journal of Aircraft, Vol. 10, No. 8, August 1973, pp. 481-486.

3. Bevilaqua, P. M., "Evaluation of Hypermixing for Thrust Augmenting Ejectors," Journal of Aircraft, Vol 11, No. 6, June 1974, pp. 348-354.

4. Fearn, R., and Weston, R. P., "Vorticity Associated with a Jet in a Cross Flow," AIAA Journal, Vol. 12, No. 12, December 1974, pp. 1666-1671.

5. DeJoode, A. D. and Patankar, S. V., "Prediction of Three Dimensional Turbulent Mixing in an Ejector," AIAA Journal, Vol. 16, No. 2, February 1978, pp. 145-150.

6. Patankar, S. V. and Spalding, D. B., "A Calculation Procedure for Heat, Mass and Momentum Transfer in Three Dimensional Parabolic Flows," International Journal of Heat and Mass Transfer, Vol. 15, October 1972, pp. 1487-1806.

7. Launder, B. E. and Spalding, D. B., "The Numerical Computation of Turbulent Flows," Computer Methods in Applied Mechanics and Engineering, Vol. 3, No. 2, March 1974, pp. 269-289.

8. Throndson, L. W., "Compound Ejector Thrust Augmenter Development" ASME Paper No. 73-GT-67.

9. Tennekes, H. and Lumley, J. L., "A First Course in Turbulence," MIT Press; Cambridge, Mass, 1972.

10. Mefferd, L. A. and Bevilaqua, P. M., "Computer-Aided Design Study of Hypermixing Nozzles," NASC Report NR78H-91, July 1978.

11. Viets, H., "Thrust Augmenting Ejectors," ARL, TR 75-0224, June 1975.